# $H_2O_2$ Assisted Room Temperature Oxidation of $Ti_2C$ MXene for Li-ion Battery Anodes

Bilal Ahmed[1], Dalaver H. Anjum[1], Mohamed N. Hedhili[1], Yury Gogotsi[2] and Husam N. Alshareef[1,*]

[1]Materials Science and Engineering, King Abdullah University of Science and Technology (KAUST), Thuwal, 23955–6900, Saudi Arabia

[2]Department of Materials Science and Engineering, and A.J. Drexel Nanomaterials Institute, Drexel University, Philadelphia, PA, 19104, USA

**Abstract**

Herein we demonstrate that a prominent member of MXene family, $Ti_2C$, undergoes surface oxidation at room temperature when treated with hydrogen peroxide ($H_2O_2$). The $H_2O_2$ treatment results in opening up of MXene sheets and formation of $TiO_2$ nanocrystals on their surface, which is evidenced by high surface area of $H_2O_2$ treated MXene and X–ray diffraction (XRD) analysis. We show that the reaction time and amount of hydrogen peroxide used are the limiting factors, which determine the morphology and composition of the final product. Furthermore, it is shown that the performance of $H_2O_2$ treated MXene as anode material in Li ion batteries (LIBs) was significantly improved compared to as-prepared MXenes. For instance, after 50 charge/discharge cycles, specific discharge capacities of 389 mAh/g, 337 mAh/g and 297 mAh/g were obtained for $H_2O_2$ treated MXene at current densities of 100 mA/g, 500 mA/g and 1000 mA/g, respectively. In addition, when tested at a very high current density, such as 5000 mA/g, the $H_2O_2$ treated MXene showed a specific capacity of 150 mAh/g and excellent rate capability.

These results clearly demonstrate that $H_2O_2$ treatment of $Ti_2C$ MXene improves MXene properties in energy storage application, such as Li ion batteries or capacitors.

**Highlights**

Room temperature oxidation of $Ti_2C$ MXene by $H_2O_2$ treatment

Preparation of $TiO_2/Ti_2C$ nanocomposite for electrochemical applications

Very good Li-ion battery performance of $H_2O_2$ treated MXenes

*Corresponding author: husam.alshareef@kaust.edu.sa

**Keywords:** MXene, $Ti_2C$, $TiO_2$, anode, lithium ion battery

## 1. Introduction

Two–dimensional (2D) atomic crystals, such as graphene, are known to possess unique properties, which lead to their applications in various emerging research areas of scientific and technological importance.[1] Over the years, 2D materials other than graphene have been developed by exfoliating layered materials such as hexagonal boron nitride,[2] metal chalcogenides ($MoS_2$, etc.)[3-6] and transition metal oxides (TMO).[7-9] Owing to their high surface area and excellent electronic properties, 2D materials are considered as potential candidates for electrochemical energy storage, hydrogen storage and thermoelectrics.

About four years ago, a new family of 2D materials transition metal carbides named as MXenes was discovered and gained significant attention due to their excellent electrochemical and mechanical properties.[10] MXenes produced by chemical etching of MAX phases, whereas MAX phases are represented by a general formula – $M_{n+1}AX_n$, where M is an early transition metal, A is an A–group element (mostly Al or Si) and X is carbon and/or nitrogen. The selective removal of A–layer by using hydrofluoric acid (HF) results in 2D layers of $M_{n+1}X_n$.[11] Due to their structural similarity with graphene, these newly formed 2D materials are termed MXenes.[10] Various members of MXene family offer metallic conductivity and surface hydrophilicity.[10] MXenes have already shown promise in supercapacitors,[12-14] Li-ion batteries (LIBs),[15-18] Li–sulfur batteries,[19] sensors,[20, 21] as filler in multifunctional polymer composites[22] and water purification.[23] In addition, theoretical studies suggest that several members of this family can become potential candidate for hydrogen storage[24] and thermoelectric[25] applications.

Typically, the exfoliated MXene sheets are terminated by –OH, -O and/or –F functional groups (marked as $T_x$) due to aqueous HF treatment and their formula is written as $Ti_2CT_x$ or $Ti_3C_2T_x$. [10]

Furthermore, it has been reported that band gap of these materials can be finely tuned by changing the nature of functional groups.[10] Also, based on density functional theory (DFT) studies, it has been predicted that bare MXene sheets have a higher theoretical capacity in Li ion batteries than terminated ones.[26, 27] In recent reports, heat treatment has been reported as an efficient way to alter the surface chemistry of MXene sheets. [28, 29] Rakhi *et. al* reported that heating $Ti_2CT_x$ in different atmospheres significantly improves its capacitive performance.[29] Naguib *et. al* reported that flash oxidation of $Ti_3C_2T_x$ MXene in air results in growth of nanocrystalline $TiO_2$ on disordered graphitic carbon sheets.[28] The resulting $TiO_2$/C composite showed promising performance when tested as anode material in LIBs. *In situ* transmission electron microscopy (TEM) revealed that either anatase or rutile nanocrystals of $TiO_2$ can be formed by controlling time, temperature and heating rate.[30] In addition, hydrothermal treatment of $Ti_3C_2T_x$ resulted in a hybrid $TiO_2/Ti_3C_2$ structure with an enhanced photocatalytic activity. The amount of produced $TiO_2$ depended on temperature and time of hydrothermal treatment.[31]

In this study, we aimed to alter the surface chemistry of $Ti_2CT_x$ MXene bysimple and scalable room-temperature oxidation in hydrogen peroxide ($H_2O_2$) solution. It resulted in the formation of $TiO_2$ nanocrystals on the surface of MXene sheets, which significantly improved the performance of the material in Li-ion battery anodes.

## 2. Experimental Section

### 2.1 Synthesis of $Ti_2CT_x$ MXene, $H_2O_2$ Treatment and Material Characterization

Chemical exfoliation of commercially available $Ti_2AlC$ (–325 mesh, Maxthal 211, Kanthal, Sweden) resulted in 2D titanium carbide ($Ti_2CT_x$) nanosheets. The exfoliation procedure was the

same as reported elsewhere[32]; $Ti_2AlC$ powder was immersed in 10% HF for 10 h at room temperature. The resulting suspension was washed with DI water and filtered to obtain 2D $Ti_2CT_x$ powder and dried at 60 °C for 24 hrs under vacuum. The as-prepared MXene powder was allowed to react with $H_2O_2$ solutions of different concentrations for different times. In a typical reaction, 0.5 grams of $Ti_2CT_x$ powder was immersed in 50 mL of water under constant magnetic stirring and 5 mL of 30 wt. % $H_2O_2$ was added afterwards. The $H_2O_2$ treated MXene powder was washed several times with DI water and dried under vacuum for 24 hours before further experiments.

The as-prepared and $H_2O_2$ treated MXene powders were characterized by using a powder X-ray diffractometer (XRD, Bruker, D8 ADVANCE) with Cu $K_\alpha$ radiation ($\lambda$ = 0.15406 nm). Raman spectroscopy was carried out using a LabRam Aramis Raman spectrometer with a diode pumped solid-state blue laser having an excitation wavelength of 473 nm. XPS studies were carried out in a Kratos Axis Ultra DLD spectrometer equipped with a monochromatic Al Kα x-ray source (hν=1486.6 eV) operating at 150 W, a multichannel plate and a delay line detector under a vacuum of $1 \approx 10^{-9}$ mbar. The survey and high-resolution spectra were collected at fixed analyzer pass energies of 160 eV and 20 eV, respectively and quantified using empirically derived relative sensitivity factors provided by Kratos analytical. Samples were mounted in floating mode in order to avoid differential charging. Charge neutralization was required for all samples. Binding energies were referenced to the C 1s peak of (C-C, C-H) bond, which was set at 284.8 eV. The data were analyzed with commercially available software, CasaXPS. The surface morphology and microstructure of as-prepared and $H_2O_2$ treated MXene powders were characterized with a field emission scanning electron microscope (FESEM, Nova NanoSEM from FEI), and a TEM (Titan $G^2$ 80-300 ST, FEI). Surface area and pore size distribution measurement was carried out

by using nitrogen as adsorbent at liquid nitrogen temperature (ASAP 2420, Micromeritics) and samples were degassed at 150 °C for 12 hours before analysis.

### 2.2 Electrochemical characterization

The working electrodes were prepared by mixing the active material ($H_2O_2$ treated MXene powder) with acetylene black (MTI, Inc.) and poly(vinylidene fluoride) (PVDF, MTI Inc) in a weight ratio of 80:10:10. The prepared slurry was uniformly pasted on a copper foil (MTI, Inc.) and dried at 80 °C for 24 hrs under vacuum. The average mass of active material after drying is ≈ 0.75 mg/cm$^2$. To assess the electrochemical performance, 2032 coin–type (MTI, Inc.) half–cell devices were fabricated. The $H_2O_2$ treated MXene powder, pasted on copper foil, served as working electrode, Lithium foil was used as counter electrode and Celgard 3501 micro porous membrane was used separator. 1 M $LiPF_6$ in ethylene carbonate (EC)/dimethyl carbonate (DMC) (1:1 by weight) was used as electrolyte. The cells were assembled in an argon–filled glove box (MBRAUN) with the concentrations of $O_2$ and $H_2O$ < 0.5 ppm. The electrochemical performance of the assembled cells was measured at different current densities (100–5000 mA/g) in the 0.005–3.00 V range. Cyclic voltammetry was performed to examine the reduction and oxidation peaks in the voltage range of 0.005 – 2.8 V (V vs. Li/Li$^+$) at a scan rate of 0.2 mV/s.

## 3. Results and Discussions

### 3.1 Material Characterization

Three different samples will be discussed in this paper: 1) As-prepared $Ti_2CT_x$, 2) $Ti_2CT_x$ treated in $H_2O_2$ for 5 minutes and 3) $Ti_2CT_x$ treated in $H_2O_2$ for 5 hours. Figure 1a shows the XRD patterns of as-prepared and $H_2O_2$ treated (5 minutes) powders. It can be readily observed that (0002) peak of $Ti_2AlC$ MAX phase shifts towards lower angles in the as-prepared $Ti_2CT_x$, which

indicates the removal of Al and increase of the *c* lattice parameter.[32] In addition, the (0002) peak, mentioned as MXene peak, broadens as compared to the sharper parent phase peak which corresponds to the decreasing structural order.[32] However small amount of residual $Ti_2AlC$ remained ion the $Ti_2CT_x$ powder. The XRD spectrum of $H_2O_2$ treated MXene powder shows the presence of anatase ($TiO_2$). A sharp peak at $2\theta \approx 25°$ corresponds to (101) plane of anatase $TiO_2$ (JCPDS card no. 00−021−1272).[29] Despite the formation of anatase, the (0002) peak of MXene phase is also present, which indicates that the resulting product is mainly MXene phase. Figure 1b shows the Raman spectra of as-prepared MXene and $H_2O_2$ treated MXene (immersion time ≈ 5 minutes) powders. The $H_2O_2$ treated MXene powder showed a major peak around 150 $cm^{-1}$, which corresponds to the anatase.[28, 33] The other three Raman bands (≈ 250, 400 and 600 $cm^{-1}$) represent the vibration modes which can be assigned to nonstoichiometric titanium carbide.[34] Furthermore, it can be observed that after $H_2O_2$ treatment the Raman band centered at 400 $cm^{-1}$ shifted towards higher wavelengths, which can be attributed to the layers emaciation.[29] As previously reported, the decrease in layer thickness shifts the band position to a higher energy due to slight hardening of the bonds.[29] Another interesting observation in Raman spectra is the absence of D and G bands after $H_2O_2$ treatment. In previous reports, when flash oxidation of MXene powder[28] was carried out, the final product was nanocrystalline $TiO_2$ supported on disordered carbon sheets due to insufficient amount of oxygen or oxidation time to oxidize carbon. However, in this case, the absence of D and G bands indicates that our final product is nanocrystalline $TiO_2$ supported on MXene ($Ti_2CT_x$) sheets. The chemical reaction of MXene oxidation in $H_2O_2$ can be written as follow:

$$a Ti_2CT_x + H_2O_2 \rightarrow b TiO_2 + (1-b) Ti_2CT_x + CO_y$$

When $Ti_2CT_x$ powder is immersed in $H_2O_2$ solution, it oxidizes to form $TiO_2$ and emits $CO/CO_2$. The nitrogen adsorption/desorption isotherms of the as-prepared and $H_2O_2$ treated MXene powders are shown in. The specific surface area (SSA) values were calculated by using Brunauer–Emmett–Teller (BET) model, where the as-prepared MXene powder showed the SSA of ≈ 12.6 $m^2/g$, while $H_2O_2$ treated MXene powder exhibited an increase in SSA to 58 $m^2/g$ (Figure S1). This fivefold increase in SSA values can be explained by the formation of $TiO_2$ nanoparticles and opening/swelling of the layers after $H_2O_2$ treatment. Figure 1c shows the SEM image of $H_2O_2$ treated MXene where layers are being opened up and $TiO_2$ formation on their surface is initiated. The XRD and Raman results presented earlier also support this conclusion.

XPS investigations were performed to characterize the chemical composition of prepared powder and to determine the oxidation state of titanium (Ti). The detailed survey spectrum for the as-prepared MXene powder shows the presence of Ti, fluorine (F), oxygen (O), and carbon (C) (Figure S2). High-resolution XPS spectra of Ti 2p and C 1s core levels from the same sample are shown in Figures 2a and 2b, respectively. The Ti 2p core level was fitted with four doublets (Ti 2p $2p_{3/2}$ – Ti $2p_{1/2}$) with a fixed area ratio equal to 2:1 and doublet separation of 5.7 eV. The Ti $2p_{3/2}$ components were located at 454.4 eV, 455.9 eV, 457.4 eV and 458.6 eV, respectively. The Ti $2p_{3/2}$ component centered at 458.6 eV is associated with Ti ions with a formal valence 4+,[35] while the peak at lower binding energy 457.4 eV is associated with Ti ions with reduced charge state ($TiO_{2-x}$).[36] The Ti $2p_{3/2}$ component centered at 454.4 eV corresponds to Ti-C bond.[36-38] The Ti $2p_{3/2}$ component centered at 455.9 eV can be assigned to the Ti-X peak in $Ti_2CT_x$ (a combination of a sub-stoichiometric $TiC_x$ (x<1) and to titanium oxycarbides $TiC_xO_y$.[39] The C 1s core level was fitted using six components located at 281.0 eV, 282.1 eV, 284.1, 284.8 eV, 286.3, 288.0 and 288.9 corresponding to C-Ti,[38, 40] C-Ti-O, C=C (sp2), C-C/C-H (sp3), C-O,

C=O[41, 42] and (O-C=O and C-F) bonds,[42-44] respectively. The survey spectrum for $H_2O_2$ treated MXene powder (immersion time ≈ 5 minutes) shows presence of Ti, F, O and C (Figure S3). High-resolution XPS spectra of Ti 2p and C 1s core levels have been obtained and presented in Figure 2c and 2d, respectively. The same fitting parameters were used to deconvolute the Ti 2p and C 1s core levels as in Figure 2a and 2b. It can be readily observed that there was a substantial decrease in the intensity of Ti $2p_{3/2}$ components at 454.4 eV, 455.9 eV and 457.4 eV for the Ti 2p spectrum accompanied with a decrease in the intensity of the C 1s component at 281.1 eV for the C 1s spectrum. This indicates that $TiO_2$ was formed at the expense of $Ti_2C$ and the ratio of titanium carbides and titanium oxycarbides to $TiO_2$ was 0.25.

Similarly, the detailed XPS spectrum for $H_2O_2$ treated MXene powder (immersion time ≈ 5 hours) also shows the presence of Ti, F, O and C (Figure S4). High-resolution XPS spectra of Ti 2p and C 1s core levels are presented in Figure 2e and 2f, respectively. The Ti 2p core level was fitted with two doublets (Ti 2p $2p_{3/2}$ – Ti $2p_{1/2}$) with a fixed area ratio equal to 2:1 and doublet separation of 5.7 eV. The Ti $2p_{3/2}$ components were located at 456.6 eV and 458.8 eV respectively. The dominant Ti $2p_{3/2}$ component centered at 458.8 eV is associated with $Ti^{4+}$ ions, while the peak at lower binding energy 456.6 eV is associated with $Ti^{3+}$ ions.[35] Interestingly, this sample didn't indicate the presence of any titanium carbides and/or oxycarbides. This result was confirmed by the high resolution XPS spectrum of C 1s core level and presented in Figure 2f. The C 1s core level was fitted using four components located at 284.8 eV, 286.4, 288.0 and 288.9 corresponding to C-C/C-H , C-O, C=O and (O-C=O and C-F) bonds, respectively. The absence of Ti-C bonds (which were expected to be observed at around 281 eV) is evident. These results demonstrate that with the extended reaction time, $Ti_2C$ is completely converted into $TiO_2$.

The morphology and microstructure of as-prepared and $H_2O_2$ treated MXene powders were investigated using TEM. Figure 3a shows a relatively low magnification TEM micrograph of as-prepared MXene powder. The stacked, layered and flake-like nature of MXene sheets can be readily observed. Figure 3b presents the high-resolution (HR) TEM image, which shows the lattice planes of MXene and some surface defects. Similar type of defects has been reported for functionalized graphene[45] and it has been proposed that these defects might act as nucleation sites for metal oxide formation.[46, 47] This idea supports our previously mentioned hypothesis that when MXene powder is placed in $H_2O_2$ environment, $TiO_2$ growth is observed on the surface of MXene sheets with its nucleation starting at defects. The selected area electron diffraction (SAED) of as-prepared MXene sample, presented in Figure 3c, shows the hexagonal symmetry of the structure. It can be concluded that the MXene powder retained the crystallinity and symmetry of parent phase – $Ti_2AlC$.[10, 32]

Figure 3d and 3e show the TEM images of $H_2O_2$ treated MXene powder (immersion time ≈ 5 minutes). The flake-like MXene morphology can be seen in Figure 3d, however, when observed at a high magnification, the $TiO_2$ nanocrystals are found to be nucleated on the surface of MXene sheets. This is a clear evidence of $TiO_2$ growth on MXene sheets which is also supported by SAED pattern, presented in Figure 3f. The SAED pattern consists of two distinct phases; MXene phase, which is evidenced by the hexagonal symmetry, and anatase $TiO_2$ which is confirmed by the appearance of diffraction rings. It should be noted that the sample prepared under the same conditions was used for electrochemical characterization. However, as mentioned earlier, there are two parameters which determine the growth rate of $TiO_2$ in $H_2O_2$; the amount of $H_2O_2$ and the reaction time. Figures 3g and 3h presents the TEM and HRTEM images of an $H_2O_2$ treated sample with prolonged immersion time (≈5 hours). It can be readily observed that almost 100%

MXene is converted into $TiO_2$ phase in agreement with our XPS data presented in Figure 2e and 2f. The size (20–100 nm) and shape of $TiO_2$ nanoparticles can be seen from Figure 3g. The HRTEM image and SAED pattern confirmed the presence of pure anatase $TiO_2$ phase. Based on HRTEM and SAED results, it can be concluded that room temperature oxidation of $Ti_2CT_x$ with $H_2O_2$ produces a hybrid structure of $TiO_2$ and $Ti_2C$.

### 3.2 Electrochemical Characterization

To assess the potential of using $H_2O_2$ treated MXene in Li–ion batteries (LIBs), we studied its electrochemical behavior with respect to $Li^+$ ion insertion and extraction. The cyclic voltammetry (CV) study of as-prepared MXene and $H_2O_2$ treated MXene (immersion time ≈ 5 minutes) electrodes was performed in the potential window of 5.0 mV to 2.8 V, at the scan rate of 0.2 mV/s and measured current–voltage (I–V) curves are presented in Figure 4a. The CV scan for as-prepared MXene matches with the previously published data,[15, 16] where two distinct oxidation and reduction peaks were observed on charging/discharging. Interestingly, the CV scan for $H_2O_2$ treated MXene is not entirely different from the as-prepared MXene, except the higher values of obtained current which, in turn, indicates a higher capacity. In addition, typical oxidation and reduction peaks for $TiO_2$ were not observed, which implies that the major capacity contribution is still coming from $Ti_2CT_x$. Thus, the observed increase in specific capacity after $H_2O_2$ treatment is mainly due to opening of layer spacing and improved accessibility of MXene surface to Li ions. When the CV scan was initiated from open circuit voltage (OCV), four distinct peaks were observed at ≈1.75 V, ≈1.30 V, ≈0.95 V and ≈0.60 V (vs. $Li/Li^+$). Two peaks among these are irreversible and do not appear in the succeeding cycles. The presence of irreversible peaks can be assigned to the formation of solid electrolyte interface (SEI) and/or reaction with the electrode material.[16] The broad oxidation and reduction peaks imply that

lithium is stored over a larger voltage range which makes it a better candidate for Li ion capacitors.[15] The CV curves for the $H_2O_2$ treated MXene (immersion time ≈ 5 hours) are presented in Figure S5. With more immersion time, the MXene sheets are fully oxidized and converted into $TiO_2$ (Figure 2e and 2f), leading to distinct $TiO_2$ lithiation/delithiation peaks in CV scans..

The galvanostatic charge/discharge curves at current densities 100 mA/g (C/3.5), 200 mA/g (C/1.75), 300 mA/g, 400 mA/g, 500 mA/g and 1000 mA/g (Figure 4b) show similar voltage plateaus (the C-rates were calculated based on theoretical capacity of $Ti_2CO_2$ ≈ 350 mAh/g). These data are consistent with the observations made using CV scans. The cyclic performance of $H_2O_2$ treated MXene at three different current densities has been measured and presented in Figure 4c. The first discharge capacity was measured as 1015 mAh/g, 826 mAh/g and 681 mAh/g at 100 mA/g, 500 mA/g and 1000 mA/g, respectively. The second discharge capacity values were 507 mAh/g, 429 mAh/g and 384 mAh/g at 100 mA/g, 500 mA/g and 1000 mA/g, respectively. Again, the irreversible capacity loss could be attributed to the formation of SEI layer or reaction of Li ions with –F and –OH groups on the surface of MXenes.[48] After 50 cycles, the observed specific capacity was 389 mAh/g, 337 mAh/g and 297 mAh/g at 100 mA/g, 500 mA/g and 1000 mA/g, respectively. These values are almost two times higher when compared with the specific capacity of as-prepared MXene at similar current densities, presented in the same figure (hollow symbols). The most probable reason is the formation of $TiO_2$ nanoparticles and improved accessibility of MXene surface after $H_2O_2$ treatment. At this stage, we won't assign this high specific capacity to the presence of $TiO_2$ because we have not observed its contribution towards capacity in CV scans or charge/discharge curves. One should note that the previously published literature also suggests that whenever surface area of MXene was increased

either by delamination[13, 49] or flash oxidation,[28] the specific capacity increased tremendously. Furthermore, the observed specific capacity of oxidized $Ti_2CT_x$ allows it to compete with the graphite anodes and suggests that partial oxidation of MXenes, which holds promise for increasing their capacity, is a valuable route for practical applications in energy storage devices.

Besides this promising gravimetric capacity and cyclic performance, $H_2O_2$ treated $Ti_2CT_x$ demonstrated excellent performance at current densities as high as 1000–5000 mA/g. After being cycled at 5000 mA/g, the cell was retested at 1000 mA/g, showed the specific capacity of 280 mAh/g at the $1000^{th}$ cycle (compared to 297 mAh/g after the $50^{th}$ cycle), indicating excellent rate performance of oxidized $Ti_2CT_x$. This ability of handle high current densities makes $Ti_2CT_x$ a suitable candidate for Li ion capacitors.

## 4. Conclusions

We have demonstrated that $H_2O_2$ treatment is a scalable and cost effective room temperature method to produce $TiO_2/Ti_2C$ hybrid materials. The presence of $TiO_2$ was observed by XRD, Raman, XPS and HRTEM. The MXene powder treated in $H_2O_2$ for 5 min showed the fivefold increase in specific surface area, as compared to as-prepared MXene powder. In addition, when $H_2O_2$ treated MXene powder was tested as anode in Li ion batteries, it showed a significantly improved performance. The excellent battery performance is mainly attributed to the higher surface area accessible to Li ions, which comes from the opening/swelling of MXene layers due to the $H_2O_2$ treatment and titania formation. Furthermore, the high rate performance and excellent cycle life make partially oxidized MXene a viable candidate for Li ion capacitors.

**Acknowledgement**

This research was supported by King Abdullah University of Science and Technology under the KAUST-Drexel University Competitive Research Grant.

**References**

1. G. R. Bhimanapati, Z. Lin, V. Meunier, Y. Jung, J. Cha, S. Das, D. Xiao, Y. Son, M. S. Strano, V. R. Cooper, L. Liang, S. G. Louie, E. Ringe, W. Zhou, S. S. Kim, R. R. Naik, B. G. Sumpter, H. Terrones, F. Xia, Y. Wang, J. Zhu, D. Akinwande, N. Alem, J. A. Schuller, R. E. Schaak, M. Terrones and J. A. Robinson, *ACS Nano*, 2015, **9**, 11509.
2. D. Pacile, J. C. Meyer, C. O. Girit and A. Zettl, *Applied Physics Letters*, 2008, **92**, 133107.
3. P. Joensen, R. F. Frindt and S. R. Morrison, *Materials Research Bulletin*, 1986, **21**, 457.
4. K. S. Novoselov, D. Jiang, F. Schedin, T. J. Booth, V. V. Khotkevich, S. V. Morozov and A. K. Geim, *Proc Natl Acad Sci U S A*, 2005, **102**, 10451.
5. B. K. Miremadi and S. R. Morrison, *Journal of Applied Physics*, 1988, **63**, 4970.
6. J. W. Seo, Y. W. Jun, S. W. Park, H. Nah, T. Moon, B. Park, J. G. Kim, Y. J. Kim and J. Cheon, *Angew Chem Int Ed*, 2007, **46**, 8828.
7. R. Ma and T. Sasaki, *Adv Mater*, 2010, **22**, 5082.
8. M. M. J. Treacy, S. B. Rice, A. J. Jacobson and J. T. Lewandowski, *Chemistry of Materials*, 1990, **2**, 279.
9. N. Takahashi, H. Hata and K. Kuroda, *Chemistry of Materials*, 2011, **23**, 266.
10. M. Naguib, M. Kurtoglu, V. Presser, J. Lu, J. J. Niu, M. Heon, L. Hultman, Y. Gogotsi and M. W. Barsoum, *Advanced Materials*, 2011, **23**, 4248.

11. M. Naguib and Y. Gogotsi, *Accounts of Chemical Research*, 2015, **48**, 128.

12. M. R. Lukatskaya, O. Mashtalir, C. E. Ren, Y. Dall'Agnese, P. Rozier, P. L. Taberna, M. Naguib, P. Simon, M. W. Barsoum and Y. Gogotsi, *Science*, 2013, **341**, 1502.

13. Y. Dall'Agnese, M. R. Lukatskaya, K. M. Cook, P. L. Taberna, Y. Gogotsi and P. Simon, *Electrochemistry Communications*, 2014, **48**, 118.

14. M. Q. Zhao, C. E. Ren, Z. Ling, M. R. Lukatskaya, C. Zhang, K. L. Van Aken, M. W. Barsoum and Y. Gogotsi, *Adv Mater*, 2015, **27**, 339.

15. J. Come, M. Naguib, P. Rozier, M. W. Barsoum, Y. Gogotsi, P. L. Taberna, M. Morcrette and P. Simon, *Journal of the Electrochemical Society*, 2012, **159**, A1368.

16. M. Naguib, J. Come, B. Dyatkin, V. Presser, P. L. Taberna, P. Simon, M. W. Barsoum and Y. Gogotsi, *Electrochemistry Communications*, 2012, **16**, 61.

17. M. Naguib, J. Halim, J. Lu, K. M. Cook, L. Hultman, Y. Gogotsi and M. W. Barsoum, *Journal of the American Chemical Society*, 2013, **135**, 15966.

18. O. Mashtalir, M. R. Lukatskaya, M. Q. Zhao, M. W. Barsoum and Y. Gogotsi, *Adv Mater*, 2015, **27**, 3501.

19. X. Liang, A. Garsuch and L. F. Nazar, *Angew Chem Int Ed*, 2015, **54**, 3907.

20. F. Wang, C. Yang, M. Duan, Y. Tang and J. Zhu, *Biosens Bioelectron*, 2015, **74**, 1022.

21. J. Zhang, W. Wang, Y. Li and D. Y. W. Yu, *Electrochimica Acta*, 2015, **185**, 76.

22. Z. Ling, C. E. Ren, M. Q. Zhao, J. Yang, J. M. Giammarco, J. Qiu, M. W. Barsoum and Y. Gogotsi, *Proc Natl Acad Sci U S A*, 2014, **111**, 16676.

23. Y. Ying, Y. Liu, X. Wang, Y. Mao, W. Cao, P. Hu and X. Peng, *ACS Applied Materials & Interfaces*, 2015, **7**, 1795.

24. Q. Hu, D. Sun, Q. Wu, H. Wang, L. Wang, B. Liu, A. Zhou and J. He, *J Phys Chem A*, 2013, **117**, 14253.

25. M. Khazaei, M. Arai, T. Sasaki, M. Estili and Y. Sakka, *Phys Chem Chem Phys*, 2014, **16**, 7841.

26. Q. Tang, Z. Zhou and P. Shen, *Journal of the American Chemical Society*, 2012, **134**, 16909.

27. A. N. Enyashin and A. L. Ivanoyskii, *Journal of Physical Chemistry C*, 2013, **117**, 13637.

28. M. Naguib, O. Mashtalir, M. R. Lukatskaya, B. Dyatkin, C. Zhang, V. Presser, Y. Gogotsi and M. W. Barsoum, *Chem Commun*, 2014, **50**, 7420.

29. R. B. Rakhi, B. Ahmed, M. N. Hedhili, D. H. Anjum and H. N. Alshareef, *Chemistry of Materials*, 2015, **27**, 5314.

30. H. Ghassemi, W. Harlow, O. Mashtalir, M. Beidaghi, M. R. Lukatskaya, Y. Gogotsi and M. L. Taheri, *Journal of Materials Chemistry A*, 2014, **2**, 14339.

31. Y. P. Gao, L. B. Wang, A. G. Zhou, Z. Y. Li, J. K. Chen, H. Bala, Q. K. Hu and X. X. Cao, *Materials Letters*, 2015, **150**, 62.

32. M. Naguib, O. Mashtalir, J. Carle, V. Presser, J. Lu, L. Hultman, Y. Gogotsi and M. W. Barsoum, *ACS Nano*, 2012, **6**, 1322.

33. V. Swamy, A. Kuznetsov, L. S. Dubrovinsky, R. A. Caruso, D. G. Shchukin and B. C. Muddle, *Phys Rev B*, 2005, **71**, 184302.

34. K. J. Cai, Y. Zheng, P. Shen and S. Y. Chen, *CrystEngComm*, 2014, **16**, 5466.

35. M. C. Biesinger, L. W. M. Lau, A. R. Gerson and R. S. C. Smart, *Applied Surface Science*, 2010, **257**, 887.

36. M. M. Ottakam Thotiyl, S. A. Freunberger, Z. Peng, Y. Chen, Z. Liu and P. G. Bruce, *Nat Mater*, 2013, **12**, 1050.

37. M. Hassan, R. S. Rawat, P. Lee, S. M. Hassan, A. Qayyum, R. Ahmad, G. Murtaza and M. Zakaullah, *Appl Phys a-Mater*, 2008, **90**, 669.

38. B. H. Q. Dang, M. Rahman, D. MacElroy and D. P. Dowling, *Surf Coat Tech*, 2012, **206**, 4113.

39. S. Zhang, Y. Q. Fu, X. L. Bui and H. J. Du, *Int J Nanosci Ser*, 2004, **3**, 797.

40. L. Guanglong, H. Changseok, P. Miguel, Z. Duanwei, L. Shuijiao, L. Vlassis, I. Nikolaos, G. K. Athanassios, F. Polycarpos, S. M. D. Patrick, J. A. Byrne and D. D. Dionysios, *Nanotechnology*, 2012, **23**, 294003.

41. F. Dong, H. Q. Wang and Z. B. Wu, *Journal of Physical Chemistry C*, 2009, **113**, 16717.

42. L. Zhang, G. Chen, M. N. Hedhili, H. Zhang and P. Wang, *Nanoscale*, 2012, **4**, 7038.

43. H. Touhara and F. Okino, *Carbon*, 2000, **38**, 241.

44. F. Y. Zhang, S. G. Advani, A. K. Prasad, M. E. Boggs, S. P. Sullivan and T. P. Beebe, *Electrochimica Acta*, 2009, **54**, 4025.

45. M. J. McAllister, J. L. Li, D. H. Adamson, H. C. Schniepp, A. A. Abdala, J. Liu, M. Herrera-Alonso, D. L. Milius, R. Car, R. K. Prud'homme and I. A. Aksay, *Chemistry of Materials*, 2007, **19**, 4396.

46. X. Wang, S. M. Tabakman and H. Dai, *Journal of the American Chemical Society*, 2008, **130**, 8152.

47. J. Xiao, D. Mei, X. Li, W. Xu, D. Wang, G. L. Graff, W. D. Bennett, Z. Nie, L. V. Saraf, I. A. Aksay, J. Liu and J. G. Zhang, *Nano Lett*, 2011, **11**, 5071.

48. Y. Xie, M. Naguib, V. N. Mochalin, M. W. Barsoum, Y. Gogotsi, X. Yu, K. W. Nam, X. Q. Yang, A. I. Kolesnikov and P. R. Kent, *Journal of the American Chemical Society*, 2014, **136**, 6385.

49. O. Mashtalir, M. Naguib, V. N. Mochalin, Y. Dall'Agnese, M. Heon, M. W. Barsoum and Y. Gogotsi, *Nat Commun*, 2013, **4**, 1716.

**List of Figures**

**TOC:**

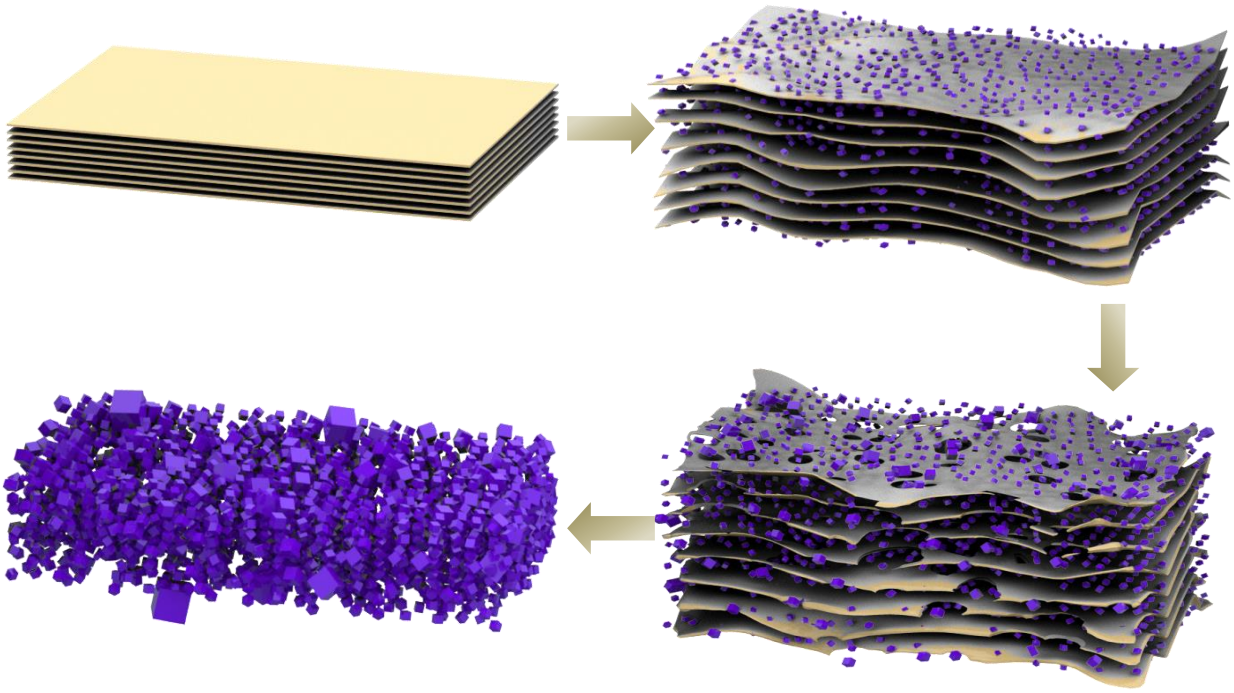

Schematic illustration of room temperature oxidation of MXene ($Ti_2CT_x$) by $H_2O_2$

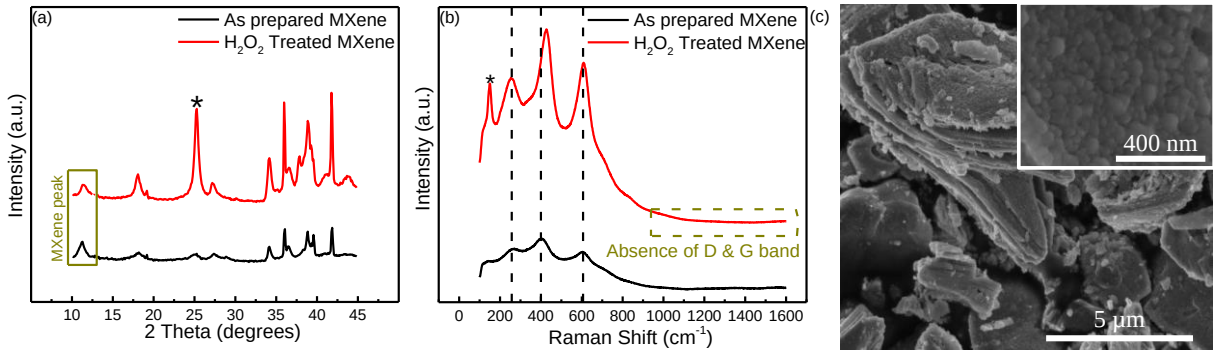


**Figure 1:** Characterization of as-prepared and $H_2O_2$ treated MXene powder (immersion time ≈ 5 minutes): (a) XRD patterns (b) Raman spectra and (c) SEM image of a typical $H_2O_2$ treated MXene flake

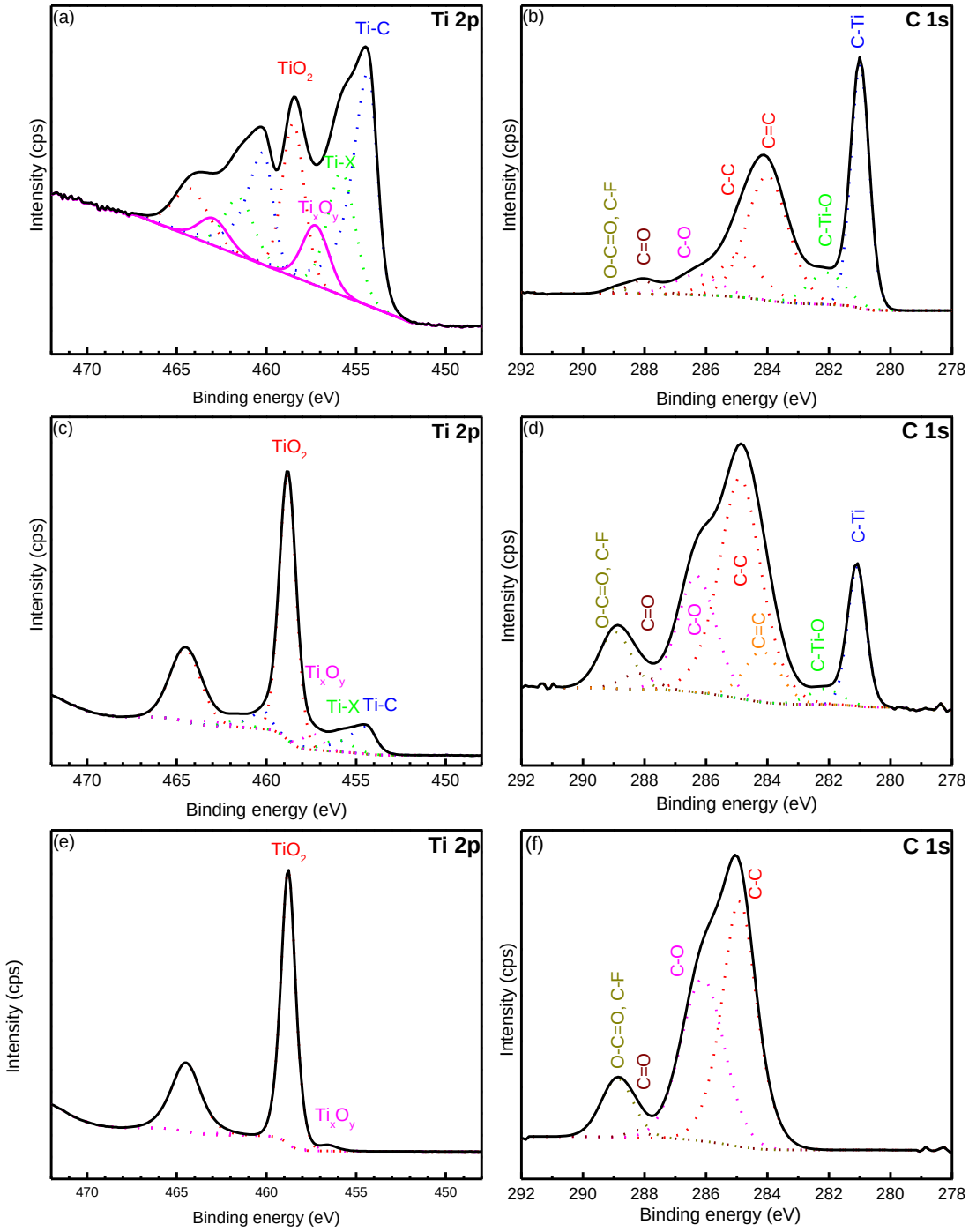


**Figure 2:** High-resolution Ti 2p and C 1s XPS spectra: (a, b) as-prepared MXene, (c–d) $H_2O_2$ treated MXene (≈ 5 minutes) and (e–f) $H_2O_2$ treated MXene (≈ 5 hours)

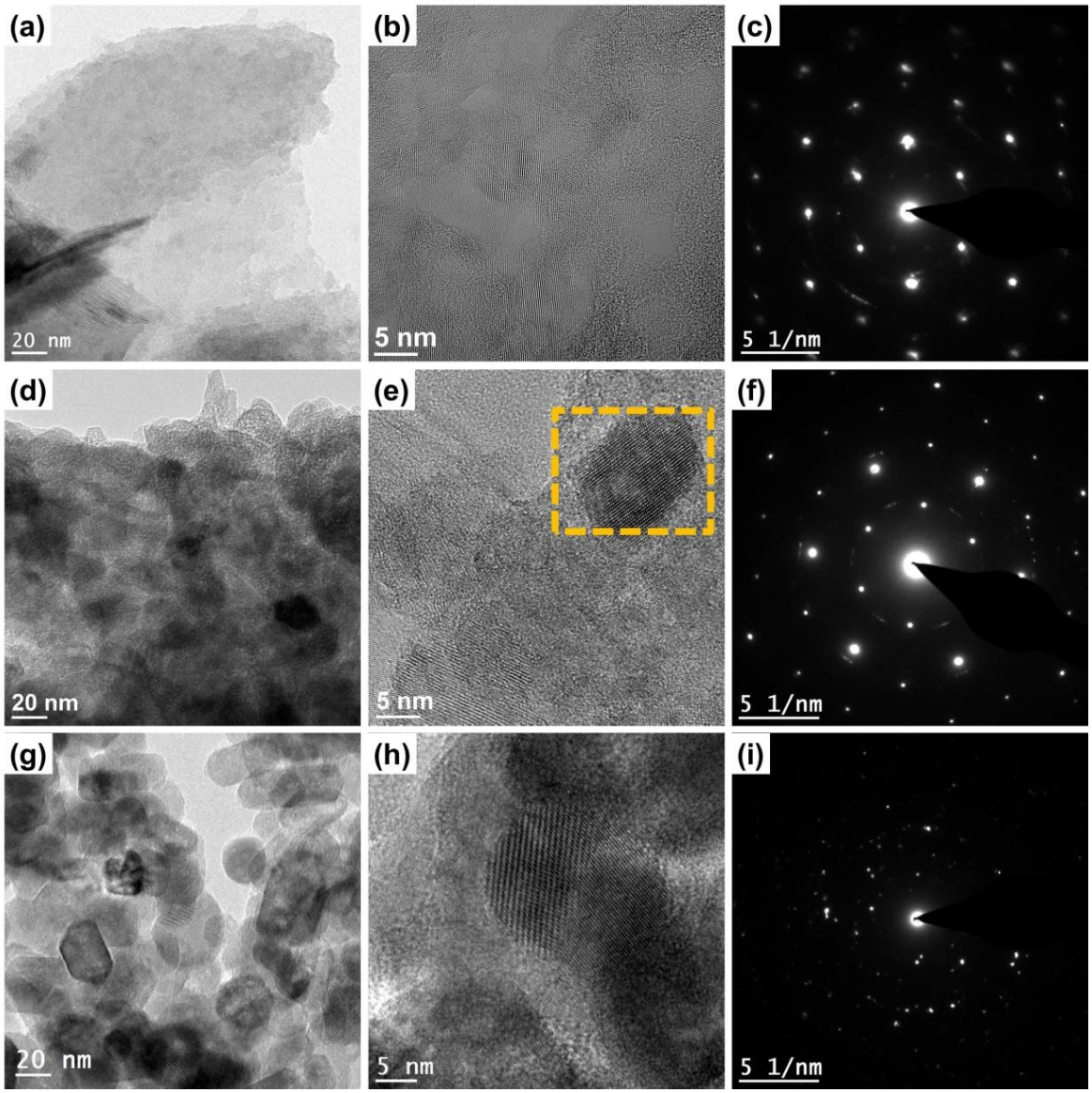


**Figure 3:** Low- and high-magnification TEM images, and SAED patterns: (a–c) as-prepared MXene, (d–f) $H_2O_2$ treated MXene (≈ 5 minutes) and (g–i) $H_2O_2$ treated MXene (≈ 5 hours)

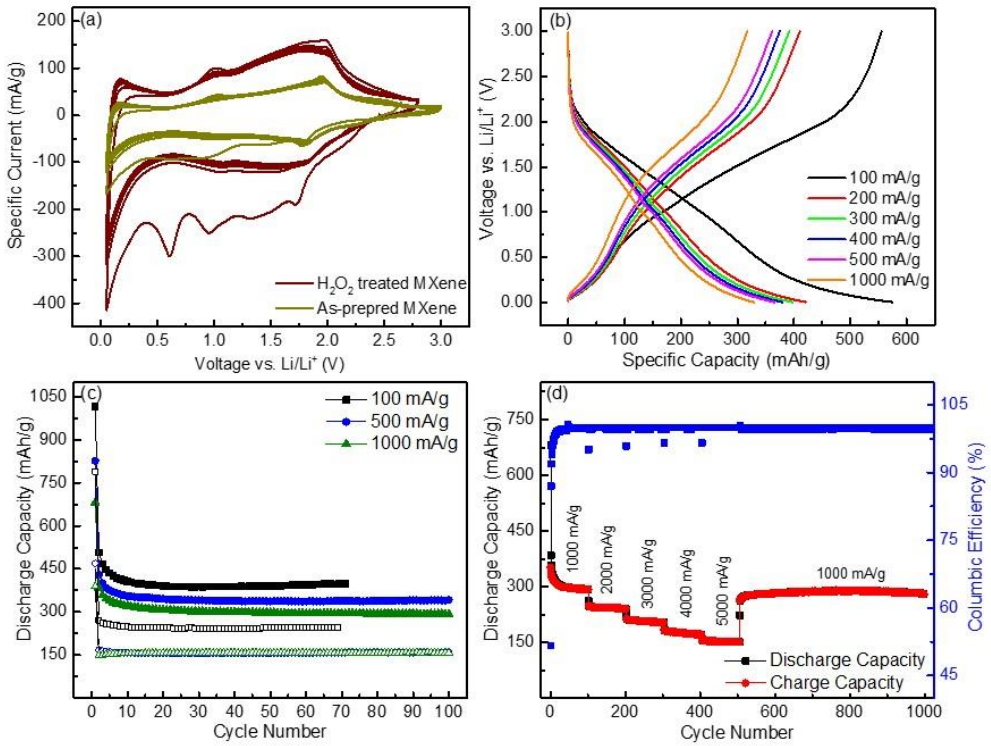


**Figure 4**: Electrochemical characterization of as-prepared and $H_2O_2$ treated MXenes (immersion time ≈5 minutes): (a) CV curves, (b) galvanostatic charge/discharge curves for $H_2O_2$ treated MXene, (c) cyclic performance at 100 mA/g (C/3.5), 500 mA/g and 1000 mA/g (solid symbols - $H_2O_2$ treated MXene; hollow symbols - as-prepared MXene) and (d) rate-ability assessment of $H_2O_2$ treated MXene (≈ 5 min) at different current densities